

Deformation in the core of a fold: Unraveling the kinematic evolution of tight, multilayer folds developed in the upper crust

Zeshan Ismat*, Bryn A. Benford¹

Franklin and Marshall College, Department of Earth and Environment, PO Box 3003, Lancaster, PA 17604-3003, USA

Received 24 January 2006; received in revised form 16 September 2006; accepted 20 September 2006

Available online 15 November 2006

Abstract

Multilayer folding models provide a framework for evaluating fold kinematics, but have limited applicability for tight folds. A careful analysis of the tight Canyon Range (CR) syncline, a natural, multilayer fold (of alternating competent quartzite and incompetent argillite layers) formed in the elasto-frictional regime, yielded the following results. (1) Fracturing and cataclastic flow occurred at multiple scales. Variations in deformation style across scales are a function of *matrix-controlled* versus *block-controlled* cataclastic flow. (2) Competent and incompetent layers switched roles in controlling fold geometry between $\sim 40^\circ$ and $\sim 60^\circ$ limb dips; models predict this switch at 60° . (3) Parasitic folds formed during later stages of fold-tightening, while most models assume that they form during early stages of folding. (4) During fold-tightening, layer-parallel shortening structures were reoriented to accommodate vertical extension.

We use multilayer folding models for initial first-order analysis of the CR syncline's kinematic history. Some of our data stray from model predictions. We use the location and timing of these variations to explain how/why the fold differs from anticipated results; this suggests critical details that may be overlooked and/or oversimplified in established folding models. Thus, kinematic details unraveled from the CR syncline improve our understanding of general multilayer fold models.

© 2006 Elsevier Ltd. All rights reserved.

Keywords: Folding; Cataclastic flow; Multilayer; Elasto-frictional; Canyon Range; Sevier FTB

1. Introduction

Natural folds can have complex geometries and kinematic histories, and relationships of fold-related structures are often not well preserved and/or ambiguous. Although physical, theoretical, and/or computer models help us understand overall development of natural folds and associated structures, they still may not be able to fully address folding complexities for two main reasons. First, few models consider the development of tight folds (e.g. Dietrich and Carter, 1969) so that existing folding models may not be applicable beyond an interlimb

angle of 100° (Ismat and Mitra, 2005b). Second, without knowing the kinematic details of a specific natural fold, models may fail to explain structures developed within that fold.

In order to improve understanding of folding processes, we conducted detailed analyses on a first-order fold, the Canyon Range (CR) syncline, in the Sevier fold-thrust belt. The CR syncline is part of an internal thrust sheet that was continuously reactivated, rather than being passively carried, as the fold-thrust belt propagated forelandward (Mitra and Sussman, 1997). So, the CR syncline records the entire history of folding in an internal sheet during the evolution of the fold-thrust belt. Because of this, results of our study have wider applicability to understanding folding in similar fold-thrust belt settings. Our study may also provide a basis for future modeling studies on fold tightening. To gain these insights, we focus on the core region of the CR syncline, where fold-tightening was accommodated by a variety of structures.

* Corresponding author. Tel.: +1 717 358 4485; fax: +1 717 291 4186.

E-mail addresses: zeshan.ismat@fandm.edu (Z. Ismat), bryn@geology.wisc.edu (B.A. Benford).

¹ Currently at University of Wisconsin-Madison, Department of Geology and Geophysics, 1215 W. Dayton St., Madison, WI 53706, USA.

The core of the CR syncline is an ideal place to study fold-tightening mechanisms for several reasons. First, the fold's core is very well exposed. Second, most of the fold-tightening occurred under shallow crustal conditions (<5 km depth) (Mitra and Sussman, 1997), within the elasto-frictional (EF) regime (Sibson, 1977; Rutter, 1986; Ismat and Mitra, 2005a), so that cross-cutting and overprinting relationships are well preserved at all scales. In the EF regime, deformation takes place primarily by fracturing and cataclastic flow, so the folding history can be unraveled by tracking fracture patterns and related structures (Mitra and Ismat, 2001; Ismat and Mitra, 2001a). Third, the CR syncline is a tight fold (interlimb angle $\sim 50^\circ$), so structures associated with tight folds can be evaluated. Finally, synorogenic conglomerates deposited in the core of the CR syncline provide temporal 'snapshots' because episodes of conglomerate deposition were coeval with fold tightening so that the conglomerates folded and fractured to different degrees as the syncline tightened.

Tracking the evolution of structures produced in a natural fold will help us better understand the complexities associated with fold-tightening, and the subtleties of folding models, which may otherwise be overlooked. We have carefully analyzed structures preserved in the core of the CR syncline in order to answer the following questions. (1) Did the kinematic evolution of the fold dramatically change beyond a certain interlimb angle? If so, how? (2) Where, at what scales, and during what stages of fold-tightening did fracturing and cataclastic flow take place? (3) What are the roles of *competent* and *incompetent* units during fold-tightening?

Answers to these questions improve our understanding of more general folding models by first locating where in the fold and at what point in its folding history the CR syncline deviated from model expectations. These observations are then used as a natural case study to determine how and why natural folds may behave in such a manner. Although models provide an excellent guide for a first-order analysis, this study attempts to reveal where weaknesses may lie in folding models. In doing this, we try to show how a natural case study can be used to strengthen and re-evaluate existing, and future, folding models.

2. Background

2.1. Folding models

Biot (1957, 1959b, 1961) and Ramberg (1960, 1963a) significantly advanced our understanding of single layer folds through a series of influential papers. However, their physical experiments using analog materials focused mainly on fold initiation. Fletcher (1977) developed additional analytical solutions for single-layer folding that extended beyond the initial increment of folding, but for low-amplitude folds. Finite element methods developed by Dieterich and Carter (1969) examined stress and strain distributions for single-layer fold shapes that ranged from low to high amplitudes. Natural rock experiments (e.g., Handin et al., 1972) and scaled physical experiments (Ramberg, 1964; Ghosh, 1966; Hudleston,

1973b; Neurath and Smith, 1982) for single-layer folds have also been studied in detail with illuminating results. Several geologists have compared the results from single-layer folding models to natural single-layer folds (e.g., Sherwin and Chapple, 1968) and have shown that these models may sometimes be misleading. Analyses on folding of *single* layers have provided critical information on the development of fold geometries, strain distribution and stress states throughout a fold. However, *multilayer* folds are more common in nature than single layer folds. Therefore, the study of multilayer folding can provide more insight into natural fold development.

Multilayer folding models typically address folding of an alternating sequence of *competent* and *incompetent* layers (Ramberg, 1964; Bayly, 1974; Summers, 1979; Williams, 1980; Cooke et al., 2000). Although these may be more realistic than single layer models (Biot, 1965; Chapple, 1969; Fletcher, 1977), they are still limited by various simplifying assumptions (Johnson, 1977; Price and Cosgrove, 1990). (1) Each layer maintains a constant flow law through time. (2) The folded multilayer sequence typically has a pinned hinge in the middle of upright, symmetrical folds. (3) The competent/incompetent fold pair does not stray far from a similar (i.e. class 2) fold shape. This implies that the competent unit maintains constant thickness and controls the fold shape while the incompetent unit behaves passively and flows from the limbs to the hinge in order to maintain contact between the alternating sequence of layers. With this type of behavior, the fold 'locks' once the fold reaches an interlimb angle of $\sim 60^\circ$ (i.e. limb dips of $\sim 60^\circ$ for symmetrical, upright folds) as the incompetent lubricant diminishes in the limbs (Dieterich, 1970; Ramsay, 1974; Williams, 1980). But clearly, there exist folds in nature whose interlimb angle is $<60^\circ$, so these models' limitations need to be relaxed and/or adjusted in order to better explain natural folding processes for tight folds.

Additionally, folds are often categorized as either *buckle* or *bend* folds, but most natural folds form as a combination of both buckling and bending processes, which may vary spatially and temporally (Ismat and Mitra, 2005b). The CR syncline initially developed, for the most part, as a 'bend' fold and continued to tighten primarily by 'buckling' (Ismat and Mitra, 2005b), but the amount of buckling and bending may have varied at different times throughout the fold. Since the CR syncline is both a buckle and bend fold, it can be used as a type natural example to understand the deformation history of folds in general, especially those that may not be as well exposed.

Our research shows that the differences between buckling and bending processes may break down once a fold reaches an interlimb angle $\sim <100^\circ$; at this point, similar types of fold-tightening accommodating structures may form in either type of fold (Ismat and Mitra, 2005b). So, irrespective of the actual mechanisms of folding (e.g. buckling, bending), the resulting strain distribution (e.g. tangential longitudinal strain, flexural slip) may be indistinguishable (Ramsay, 1967; Hobbs et al., 1976; Lisle, 2000). Here we focus our attention on the *geometry* of the fold, since this is what can be observed, in order to develop a kinematic model for folding.

2.2. Cataclastic flow

Cataclasis involves fracturing and sliding along fracture-bound clasts, or ‘blocks’. If fracturing and sliding are penetrative at a given scale and a rock body appears to deform by bulk flow, then deformation is referred to as cataclastic flow (Hadi-zadeh and Rutter, 1983; Hirth and Tullis, 1994; Ismat and Mitra, 2001a). Thus, smaller scale fracturing can produce larger-scale ductile deformation (Sibson, 1977; Hirth and Tullis, 1994; Marshak et al., 1982). Cataclastic flow is a type of ductile deformation that takes place by elasto-frictional mechanisms, generally at shallow crustal levels.

Cataclastic flow is traditionally defined for deformation at the microscale and is often assumed to not account for a significant portion of the deformation (see discussion by Elliott, 1976a). Moreover, it is implied that cataclastic flow requires a significant amount of matrix in order for the fractured clasts/blocks to slide past one another. However, cataclastic flow is capable of producing large amounts of deformation (Wojtal, 1989) and can occur at a wide range of scales, with or without matrix. Non-matrix supported cataclastic flow is referred to here as ‘block-controlled’ cataclastic flow (Ismat and Mitra, 2001a, 2005a).

Both matrix- and block-controlled cataclastic flow can take place in the same deforming system, but may vary spatially and temporally. Although the style of cataclastic flow may vary at different scales, both types assist each other in the overall deforming rock mass. Because of this, we say that there is a cooperative relationship between the two types of cataclastic flow.

In matrix-supported cataclastic flow, the clast size progressively decreases with continued deformation. During block-controlled cataclastic flow, however, the fracture-bound block size can increase or decrease; deformation cycles between fracturing and then sliding along all or some of the fractures. At each stage of frictional sliding, new and/or older reactivated fractures may be used in block-controlled cataclastic flow (see Ismat and Mitra, 2005b, Fig. 1).

3. Geology

3.1. Regional geology

The Sevier fold-thrust belt (FTB) is part of the North American Cordillera and is subdivided into salients and segments separated by recesses and transverse zones (Fig. 1). The Central Utah segment is the type area of the Sevier FTB (Christiansen, 1952; Armstrong, 1968; Mitra, 1997) (Fig. 1), and includes, from west to east, the Canyon Range (CR), Pavant (PVT), Paxton (PXT), and Gunnison (GUN) thrusts (Fig. 2) (Allmendinger et al., 1983; DeCelles et al., 1995; Mitra, 1997).

The CR thrust sheet is an internal thrust sheet in the Central Utah segment. Motion along the Pavant, Paxton, and Gunnison thrusts reactivated the CR thrust and progressively folded the CR thrust sheet into an anticline–syncline pair; this fold pair is exposed in the Canyon Mountains (Figs. 2, 3a). The

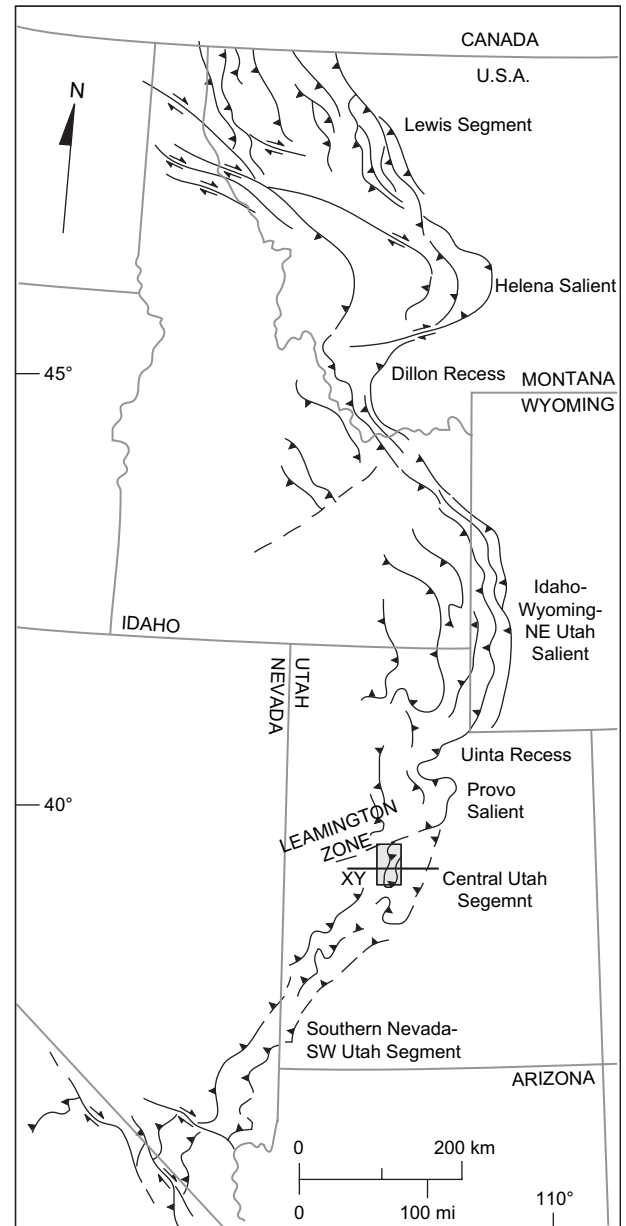


Fig. 1. The Sevier FTB of western USA, showing major salients, segments and recesses, and the transverse zones bounding them. Cross-section drawn along line XY illustrated in Fig. 2. Boxed area shows location of Fig. 3a.

thrust sheets carried by Sevier age thrusts were later broken up by Tertiary Basin-and-Range normal faulting (Fig. 2). Sevier age structures are well preserved in normal-fault bound ranges, such as the Canyon Range. These normal faults are far enough away from the CR anticline–syncline pair so that fault-related structures do not obscure the earlier Sevier aged patterns (Ismat and Mitra, 2001a, 2005a).

3.2. Stratigraphy of Canyon Range thrust sheet

The CR thrust sheet consists primarily of Proterozoic and Cambrian quartzites (Fig. 2). The major quartzite units within the CR thrust sheet are the Neo-Proterozoic Pocatello (PCp),

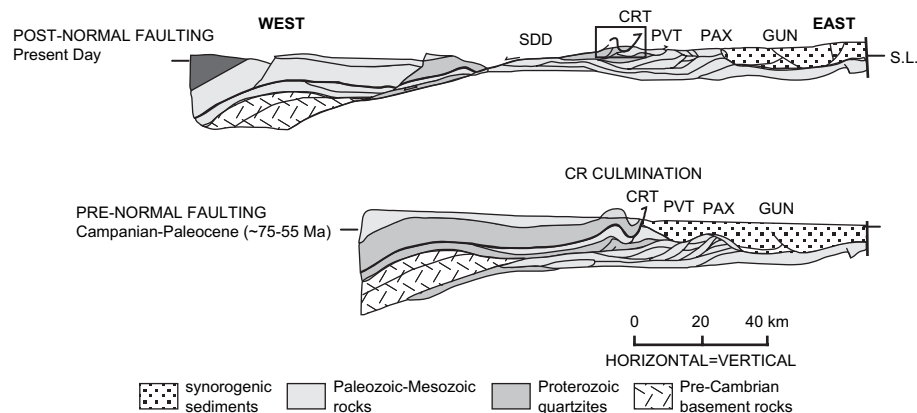


Fig. 2. Regional cross-sections drawn along line XY in Fig. 1 showing geometry after Sevier thrusting (i.e. pre-normal faulting) and present-day geometry after Tertiary Basin-and-Range normal faulting. Canyon Range thrust (CRT), Pavant thrust (PVT), Paxton thrust (PAX), Gunnison thrust (GUN) and the Sevier Desert Detachment (SDD), a low angle normal fault, are shown. Boxed area on 'present day' cross section shows location of Fig. 3a. (Cross-section modified from Mitra and Sussman, 1997.)

Caddy Canyon (PCc), and Mutual (PCm) Formations, the Eo-cambrian Tintic Formation (Ct) (lower, middle, and upper), and the Cambrian Pioche Formation (Cp); Cambrian carbonates overlie these quartzites (Christie-Blick, 1982; Hintze, 1988) (Fig. 3a). Synorogenic Cretaceous conglomerates (CR conglomerates) were deposited unconformably in the core of the CR syncline, i.e. on top of the Cambrian carbonates. The carbonate units are not exposed in part of the east- limb and hinge region of the CR syncline (Fig. 3b,c), possibly due to a transverse fault in the hinge region (Fig. 3b). So, the synorogenic conglomerates are in contact with the top of the Pioche unit in much of the core of the CR syncline (Fig. 3b,c). An intraformational conglomerate composed of fractured and cataclastic Pioche quartzite is found along this contact, in a few places, close to the hinge zone.

The core of the syncline is defined by the upper Tintic, the Pioche and the CR conglomerate; this paper focuses on the Pioche unit and the CR conglomerate, where much of the deformation is localized and well exposed (Fig. 3b,c). The Pioche is a quartzite-argillite interbedded unit; there are two primary quartzite layers, separated by an argillite layer, exposed in the CR syncline. Many small-scale structures that developed in the core are a function of the alternating lithological characteristics in the Pioche Formation.

3.3. Local geology

The Canyon Mountains' anticline–syncline pair trends approximately north-south; the west limb of the syncline and the east limb of the anticline are a common limb (Figs. 2, 3b). This fold pair formed with an overall east-west, sub-horizontal shortening direction (Ismat and Mitra, 2001a). The syncline fold tightened primarily by thinning, stretching and rotation of the west limb, and by hinge migration (Mitra and Sussman, 1997). As the anticline–syncline pair tightened, sediments eroded from the anticline were deposited unconformably into the core of the adjoining syncline, forming the CR conglomerate (DeCelles et al., 1995; Lawton et al., 1997).

The CR syncline had a protracted history that likely included early folding at deeper (~10 km) levels, followed by unroofing, and fold-tightening simultaneous with conglomerate deposition at much shallower levels (Ismat and Mitra, 2005a). Much of the fold-tightening took place during the later part of the Sevier orogeny under an overburden of ≤ 5 km, which included ~2 km of overlying synorogenic CR conglomerate (Fig. 2). Because of its shallow depth (i.e., within the EF regime), fracturing and cataclastic flow accommodated much of the CR fold-tightening (Ismat and Mitra, 2001a, 2005a). Since the conglomerates were deposited during fold-tightening, they are also tightly folded and fractured. Variation of folding between different conglomerate layers is used to track the folding history of the CR syncline. The plunge and interlimb angle for each successive folded conglomerate layer decreases, which suggests progressive steepening of the CR syncline's plunge during fold-tightening (Lawton et al., 1997).

The core of the CR syncline is well exposed at the northern end of the range and has a fold axis that plunges 32° , 337° (Fig. 3b,c). This portion of the syncline is where most of the fold-tightening occurred, and therefore, the most complex structures developed. Some of these fold-tightening related structures include parasitic folds, out-of-core thrusts, and bed thickness changes from the hinge to the limbs.

4. Data collection

To more completely understand the deformation mechanisms that took place in the CR syncline, structures related to fold-tightening were studied and documented at the macro-, meso-, and microscales.

4.1. Macroscale structures

US Geological Survey 1:24,000 topographic maps and US Forest Service aerial photographs were used to locate field sites and map macroscale patterns (Fig. 3b). The resolution of these maps was too low to accurately trace out some

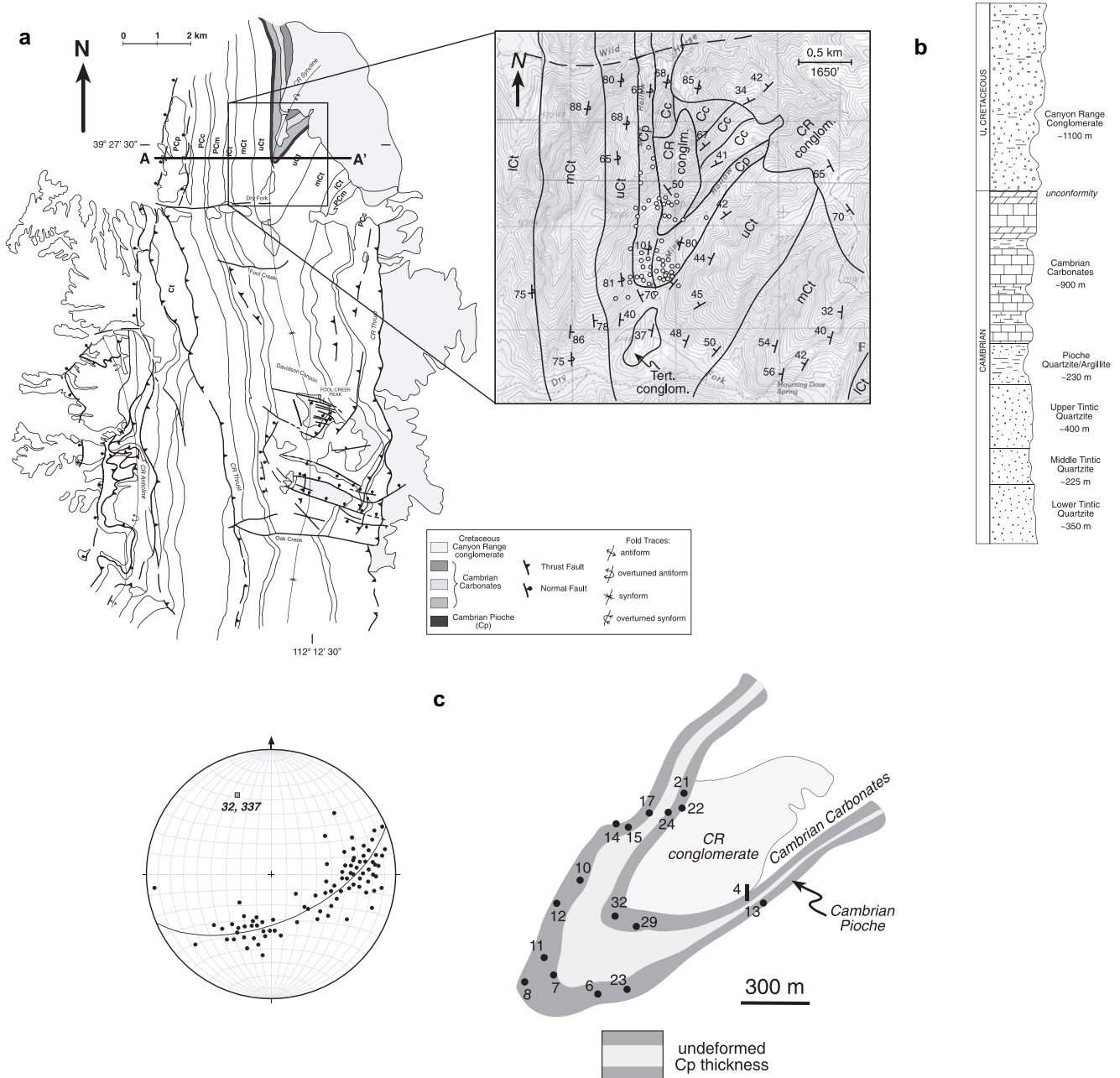


Fig. 3. (a) Geologic map of the Canyon Range (CR) anticline–syncline pair (modified from Ismat and Mitra, 2005a). The CR anticline is an antiformal-stack duplex structure. (b) Enlarged map view (on a 1:24,000' topographic map base) and stratigraphic column. The Cambrian Pioche Formation (Cp) and the Cretaceous CR conglomerate are shaded gray and white, respectively. Transverse zone is shown as a dashed line in the upper right corner. Locations where detailed field analysis was conducted are shown as white dots. (c) Down-plunge projection of shaded area from part (b) and π -diagram of bedding poles (lower hemisphere projection) measured within a ~ 1 km zone on either side of cross-section line AA' shown in part (a).

structures and contacts recognized on the ground. Because of this, photographs of the fold-core and surrounding area were taken from a low-flying light aircraft, which provided oblique views of the fold ranging from a scale of $\sim 1:10,000$ to $\sim 1:5000$. These oblique aerial photographs were used in conjunction with the topographic map, ortho-aerial photographs and the outcrop (meso) scale patterns observed on the ground, bridging between map and mesoscales of observation. From these maps and photographs, we traced out the Tintic/Pioche (Ct/Cp) and the Cp/CR conglomerate contacts. Fold-related

faults, a detailed geometry of the folded CR conglomerate and the fracture patterns within the conglomerate, are well expressed in the low altitude photographs.

4.2. Mesoscale structures

Within the CR syncline, detailed outcrop-scale field analysis was conducted at 57 sites throughout the upper-Tintic quartzite, the Pioche Formation, and the Cretaceous CR conglomerate (Fig. 3b). The fracture patterns are well represented

at a 1 m² scale. At each site, oriented rock samples were taken, and orientations of bedding and fracture sets were recorded along two mutually perpendicular 1 m² faces, in order to document the three-dimensional outcrop-scale fracture patterns. Data from a transect, ~10 m long, across the east limb into the core of the syncline were collected (Site 4, Fig. 3c), to document how the deformation changed from the limb to the core, i.e. did the fracture patterns continue into the conglomerate from the Pioche, did they refract, and did they change in density. Because fold-tightening occurred primarily by rotation, thinning and stretching of the west limb, many of the field sites were deliberately chosen in the west limb (Fig. 3b,c).

Fractures in the Pioche quartzite are mutually crosscutting and therefore interpreted to have formed concurrently at one stage of deformation. At each site, fractures were weighted according to their frequency, thickness and continuity within the site area (see Ismat and Mitra, 2001a for a more detailed description of this method). The orientations of poles to these fractures were plotted on equal-area stereonet. Great circles drawn from the pole concentrations represent the most common fracture sets, and these show conjugate-conjugate patterns. The acute bisector of these patterns gives the maximum shortening direction at each site (Reches, 1983) (Figs. 3c, 4). Slickensides are preserved on a few fracture sets in the quartzite beds of the west limb. The orientation of these slickensides and the lineations were used to determine motion planes (M-planes) at various sites (Figs. 3c, 5a) (Marshak and Mitra, 1988).

Detailed bedding and fracture data were also collected and analyzed from mesoscale second-order folds, which are all found in the Pioche quartzite (Figs. 3c, 5b). A west-directed, small (meter scale) fault-propagation fold (FPF) is preserved in the eastern portion of the hinge region of the upper quartzite layer (site 29, Figs. 5b, 6a,c), and a 5 m scale z-fold (looking north) is found in the east limb of the lower quartzite layer (Site 6, Figs. 5b, 6a). Additionally, a synformal hinge (20 m scale, i.e. much larger than either the FPF or z-fold) is well exposed within the east limb of the CR syncline in the lower Pioche quartzite layer (Site 23, Figs. 3c, 6a), just east of the z-fold.

4.3. Microscale structures

Over 40 oriented samples were collected from 30 sites within the Pioche quartzite for microstructural analysis. Most of the oriented samples were cut parallel to the east-west transport direction; ten samples were cut along three mutually perpendicular sections (vertical east-west, vertical north-south, and azimuthal plane) in order to unravel the three-dimensional deformation at the microscale. Thin sections were viewed in plane and polarized light and using dark field microscopy. In dark field, many of the structures, such as healed fractures, that were not noticeable under cross and/or plane polarized light became visible (Fig. 7).

The style of fracturing, variation in fractured clast size, and morphological characteristics of the clasts were documented in order to understand EF behavior at the microscale. These

observations were compared to features preserved at the meso and macroscale in order to determine (1) if the style of deformation continues across scales and (2) if/how the deformed rocks interacted across scales.

5. Data analysis and interpretation

5.1. Macroscale analysis

The Pioche Formation (in the CR syncline) has an undeformed thickness of ~230 m (Hintze, 1988) (Fig. 6a,b). Based on the down-plunge projection of the core of the CR syncline, we see that the hinge of the fold has a maximum thickness of ~430 m while the thinnest portions of the limbs are only ~70 m thick. So, the hinge thickened by as much as 90% while the limbs thinned by as much as 70% (Figs. 3c, 6a,b). This change in bed thickness from the hinge to the limbs may have induced the formation of complex structures in the core of the fold.

Assuming that the inner arc of the Pioche fold shortened and the outer arc extended, there should be a neutral surface (NS) between these two regions. We have drawn the NS through the middle of the fold profile, and have estimated its length to be 3000 m (Fig. 6a). Using this line length and the undeformed thickness of 230 m, the undeformed area of the Pioche Formation comprising the fold is calculated to be 6.9×10^5 m² (Fig. 6b). The measured area of the Pioche fold profile is 6.3×10^5 m² (Fig. 6a). There is less than 10% discrepancy between the undeformed and folded profile; some of this variation may simply be a function of where the NS was placed on the fold profile. Based on this small discrepancy, we surmise that there is a minimal amount of deformation in and out of the profile plane.

Synorogenic conglomerates were deposited and progressively folded as the CR syncline was tightening (Fig. 8a). The hinge for the folded conglomerate layers progressively migrates into the east limb of the CR syncline, which suggests that the depocenter shifted eastward (Fig. 8a,b). This eastward shift can only happen if the hinge of the Pioche fold migrated westward relative to the conglomerate hinges (Fig. 8a). So, evidence for hinge migration is preserved in these folded synorogenic conglomerates.

Folding of the conglomerates was accomplished by EF mechanisms. Three major sets of steeply dipping (~vertical) penetrative fractures (striking east-west, north-south, and S 30° W) are preserved within the folded synorogenic conglomerate, and define ~8 m³ fracture bound blocks (Fig. 9a). This suggests that the conglomerates may have at least partially folded by these fractured blocks sliding past one another, i.e. by block-controlled cataclastic flow (Ismat and Mitra, 2005b). The east-west trending fractures are slightly longer and more open; they crosscut the two other fracture sets and also crosscut folds in the conglomerate, and so most likely formed during the later stages of fold-tightening (Fig. 9a,b). The conglomerate has a lower fracture density than the adjacent quartzite, as some of the deformation may have been accommodated by the conglomerate's weak matrix.

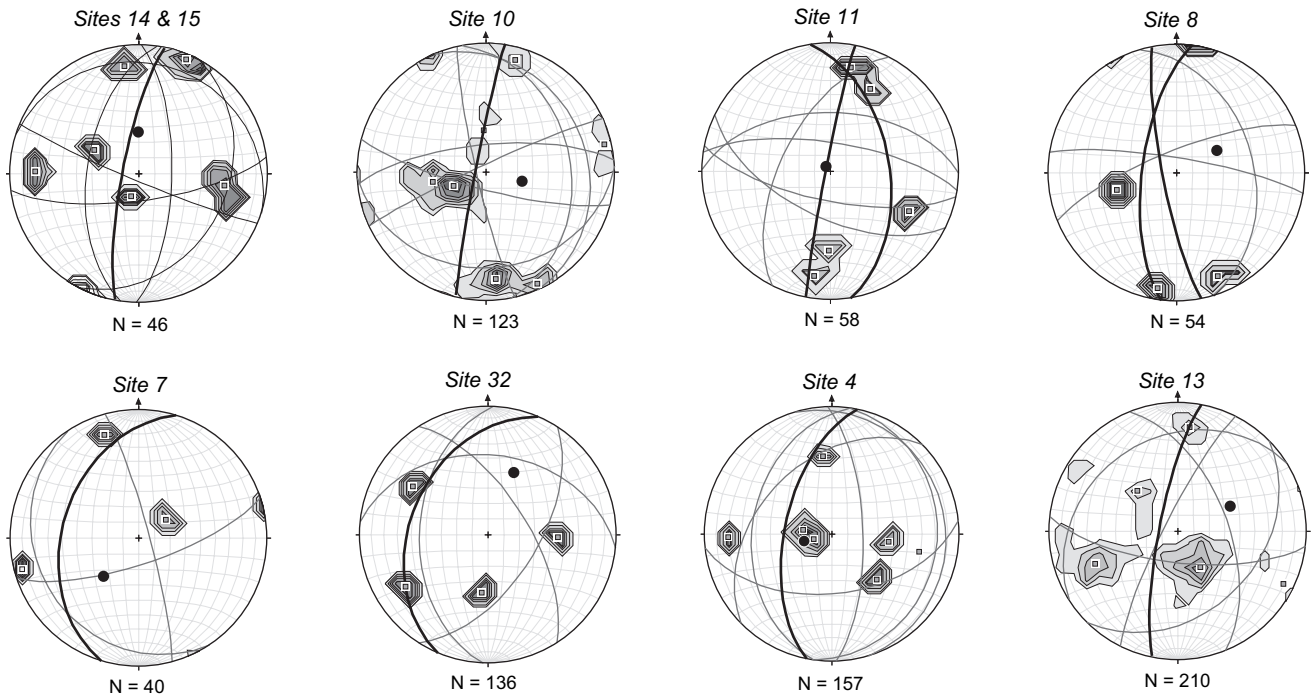


Fig. 4. Representative stereograms of fracture networks from within the quartzite layers of the Pioche Formation. Fractures were weighted and plotted as contoured poles (1% area contours) to fractures on equal-area stereonets (lower hemisphere projections). Average fracture sets, determined from the pole concentrations, are plotted as great circles. Maximum shortening (or extension, depending on the orientation of the limb) directions (black dots) are determined from the conjugate–conjugate fracture sets. Bedding for each site is represented as a thick black great circle.

Larger faults that cross-cut the entire fold core (in map view) are also preserved (Fig. 8b). These macroscale faults are steeply dipping and have an overall east-west trend. In detail, the trends of these faults change across lithologic boundaries, most likely indicating refraction during fracture propagation (Treagus, 1983; Atkinson, 1989). The ~E-W trending faults cross-cut all of the folds and fracture sets preserved in the conglomerate, and so are the youngest structures in the core. The steeply dipping, east-west trending, large faults and smaller fractures may be a result of N-S extension parallel to the hinge during fold-tightening with an overall east-west maximum shortening direction. This possibility suggests that the deformation is not entirely plane-strain. So, the ~10% discrepancy in the measured area, although small, may in fact be real.

5.2. Mesoscale analysis

Structures preserved at the mesoscale not only reveal more details than the macroscale structures on how the CR syncline fold-tightened and alleviated space problems, but also provide critical timing information for the development of certain structures. This allows for a more complete reconstruction of the CR syncline as it continued to tighten, and challenges existing folding models.

5.2.1. Hinge migration

In addition to the folded synorogenic conglomerates, the synformal hinge preserved in the east limb of the lower Pioche

quartzite is a key element in tracking the history of hinge migration in the overall CR syncline (Figs. 6a, 10). The eastern synformal hinge and the tight, first-order hinge of the CR syncline define a subdued double-kink box-fold geometry in the Pioche unit. Two possible models for the origin of this eastern synformal hinge and the resulting box-fold geometry are given below.

An existing kinematic model for the CR syncline suggests that as the fold tightens, the older hinge progressively migrates into the steepening west limb and is unfolded, and a new hinge forms farther to the east (Mitra and Sussman, 1997; Ismat and Mitra, 2001a). Based on this first model, the eastern synformal hinge is the *youngest* and the western, tight hinge represents an older hinge that was in the process of ‘unfolding’ into the west limb (Bayly, 1974). Thus, the box-fold shape preserves a ‘snapshot’ of the hinge migration process (Fig. 10a).

The second model, presented here, suggests the opposite scenario for the following two reasons. First, the orientation of the eastern synformal hinge (34° , 333°) is nearly identical to that of the first-order (western) hinge (32° , 337°), which implies that the eastern synformal hinge formed early, possibly coeval with the first-order hinge (Fig. 10). In other words, both hinges were present during the CR syncline’s entire folding history; the eastern hinge is most likely a ‘relict’ hinge of the CR syncline and the western, tight hinge is the most recently active. Second, based on detailed work within the Appalachian Valley and Ridge province, R.P. Nickelsen (1993, personal communication) has suggested that single hinge folds composed of thin layers of alternating competent

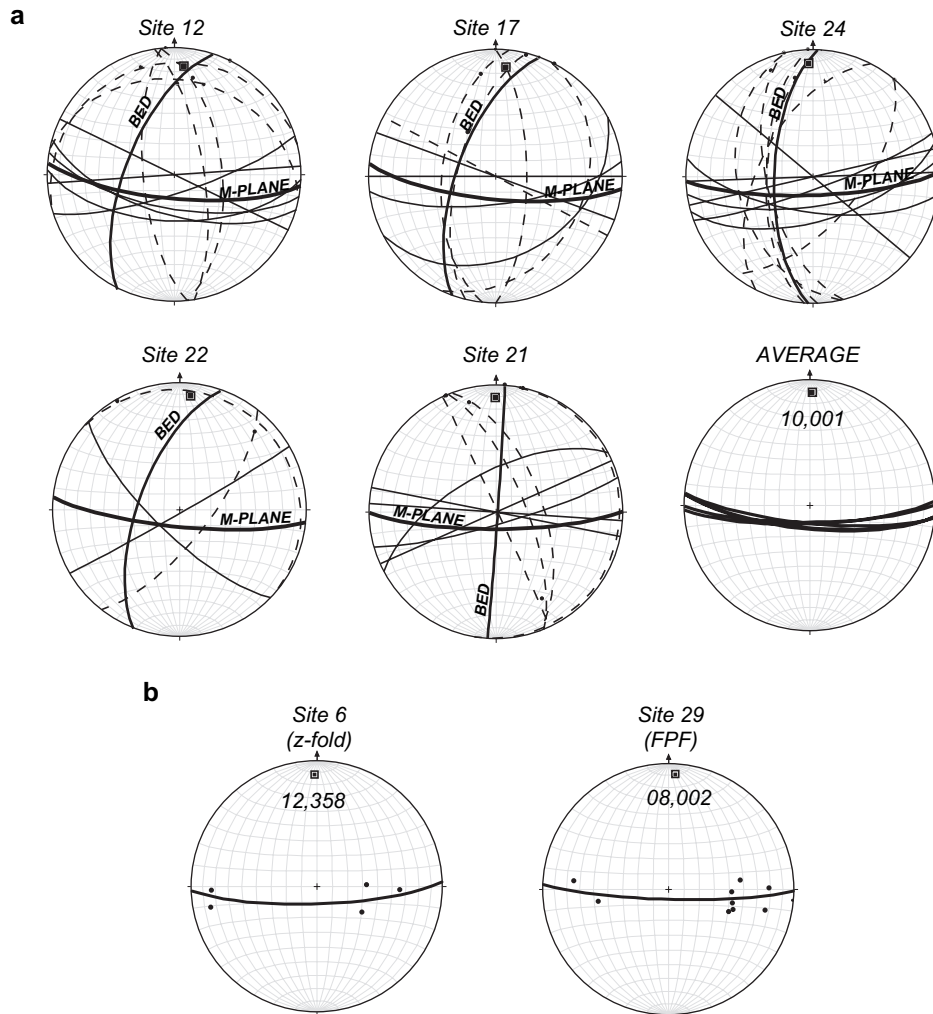


Fig. 5. (a) Motion planes from five representative sites in the Pioche quartzite unit of the west limb plotted on equal-area stereonets (lower hemisphere projections). Motion planes are constructed from the pole to the slickenside fracture surface and the lineation (slickenline) on that surface. Slickensides at each site are shown as dashed great circles. The motion plane for each fracture is shown as a thin, solid great circle. Poles to these motion planes (i.e. m-poles) are plotted as small black dots. The average motion plane at each site is obtained from the maximum concentration of m-poles and is illustrated as a thick, black great circle; its pole is shown as a square. The average motion plane and m-pole from all five sites combined is illustrated on a separate stereogram. (b) π -diagrams (lower hemisphere projections) of the parasitic z-fold and second-order fault-propagation fold (FPF) preserved in the Pioche quartzite. Site 6 is a z-fold (looking north) preserved in the lower Pioche quartzite and site 29 is an FPF (looking north) preserved within the upper Pioche quartzite. Poles to bedding (small black dots) define a great circle whose pole gives the orientation of the fold-axis. Both second-order folds' orientations are similar to each other and are similar to the average m-pole orientation.

and incompetent beds, such as the Pioche unit, may originate as double-kink box-folds. As folding progresses, only one of the hinges remains active and continues to tighten, while the other hinge is often cryptically preserved in a limb. So, in the case presented here, the eastern synformal hinge is the relict hinge of an initial, more obvious, double-kink box-fold (Fig. 10). In addition to this, earlier work in adjacent stratigraphic units suggests that the CR syncline formed as a symmetrical fold up to an interlimb angle of $\sim 100^\circ$ (i.e. 40° limb dips), at which point the west limb continued to rotate (Fig. 8a) (Ismat and Mitra, 2005b). So, the east limb maintains a dip of $\sim 40^\circ$ along the strike of the syncline. Based on this 40° limb dip, if the structure in the Pioche began as a symmetrical double-kink fold, each hinge would have had an interlimb angle of 140° (i.e., interlimb angle of 100° for the fold as

a whole) (Fig. 8a). The interlimb angle of the relict synformal hinge is 132° , very close to 140° (Fig. 10). So, the relict hinge in the Pioche quartzite did not unfold, as the other quartzite units did in the first model, but is interpreted to represent the inactive hinge of an original double-kink box-fold (Figs. 8a, 10).

Although the eastern synformal hinge may be a 'relict' feature, the interpretation of its kinematic evolution does not invalidate the earlier proposed hinge migration model for the rest of the CR fold. It does, however, suggest that the geometry and pattern of hinge migration may vary up and down through a folded sequence and this variation may be a function of lithology. In the older (Proterozoic) quartzite units that make up the bulk of the CR syncline, there are no weak horizons separating the thick, massive quartzite beds (Fig. 3a,b) and

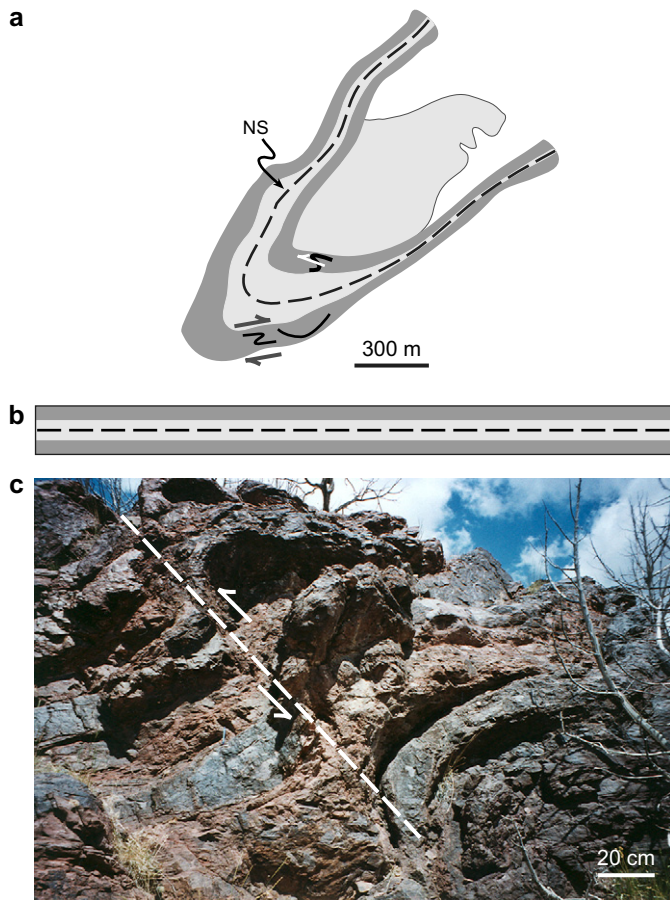


Fig. 6. (a) Down-plunge projection of the core of the CR syncline showing the synformal hinge preserved at site 23, the z-fold at site 6 and an FPF exposed at site 29 (see Fig. 3c for site locations). The scale of the two second-order folds and the synformal hinge are directly comparable. Dashed line in parts (a) and (b) represents the neutral surface (NS). (b) Undeformed dimensions of the Pioche unit. (c) Photograph of the FPF preserved at site 29, looking towards 335°.

the folding history suggests that the hinge migrated eastward as the older hinges moved into the steepening west-limb and were unfolded (Mitra and Sussman, 1997). The Pioche in the fold-core, however, is made up of two thin quartzite layers separated by a thick argillite layer and folding evolved differently in these rocks. The hinge in the Pioche fold migrated to the west as the eastern-most hinge of the double-kink box-fold moved into the east-limb of the first-order fold.

5.2.2. Bed thickness changes

The conjugate–conjugate sets of fractures preserved throughout the Pioche quartzite (including within the parasitic folds) are at low angles to bedding. This orientation suggests that they formed when the beds were sub-horizontal, accommodating layer-parallel shortening (LPS) (Figs. 4, 11a,d). These LPS fracture sets are not cross-cut by other sets of fractures, so no (or, very few) new fracture sets formed during fold-tightening. As the beds rotated with progressive fold-tightening, the conjugate–conjugate fracture sets were passively rotated and selectively reactivated to accommodate

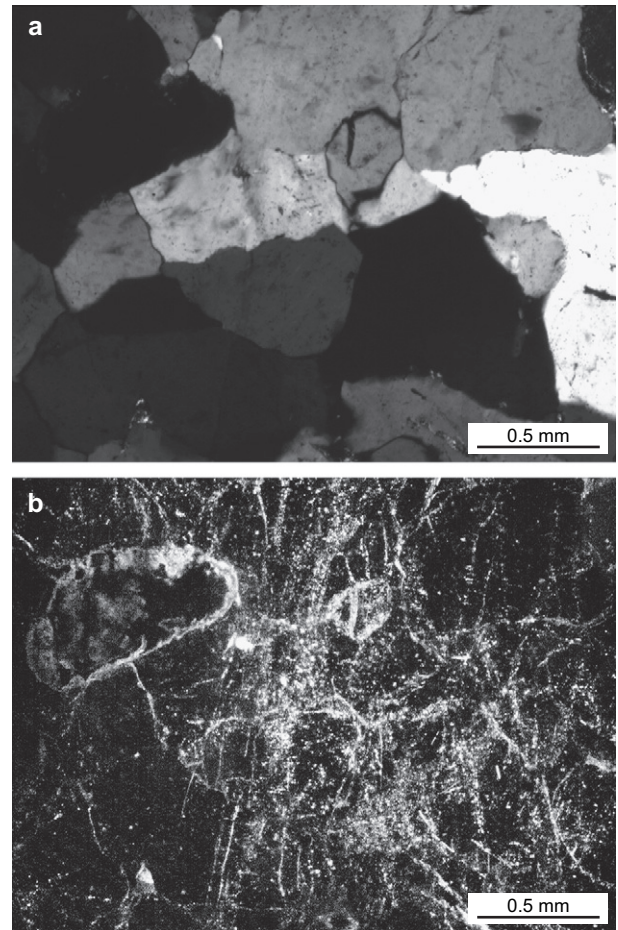


Fig. 7. Photomicrograph of non-fractured Pioche quartzite viewed under (a) cross-polars and (b) dark-field. Dark-field view highlights old grain boundaries and healed fractures.

thinning and vertical stretching of the limbs, while fractures in the hinge region continued to accommodate shortening and thickening of the beds (Figs. 3c, 4). Thus, the conjugate–conjugate fracture sets accommodated these bed thickness changes by block-controlled cataclastic flow.

After the CR syncline's limbs reached dips of $\sim 40^\circ$, folding continued by rotation of the west limb (Fig. 11d) (Ismat and Mitra, 2005b). Based on the two-dimensional model illustrated in Fig. 11d, between limb dips of 40° and 60° (i.e., between interlimb angles of 100° and 80°), only two sets of fractures in the quartzite member were 'active', i.e. sliding took place on only two fracture sets. Therefore, cataclastic flow was not an effective means of three-dimensional deformation (i.e. limb rotation) in the competent quartzite limbs during these fold stages.

The model illustrated in Fig. 11d shows that three sets of cleavage surfaces in the west limb of the Pioche fold, however, were in positions for reactivation between 40° and 60° limb dips (Fig. 11b,d). The argillite also deformed by cataclastic flow; rather than sliding along fracture surfaces, early LPS cleavage surfaces defined rhomb shaped blocks that slid past one another (Fig. 11b,c). So, pre-existing surfaces were reactivated in the argillite to accomplish fold-tightening, rather

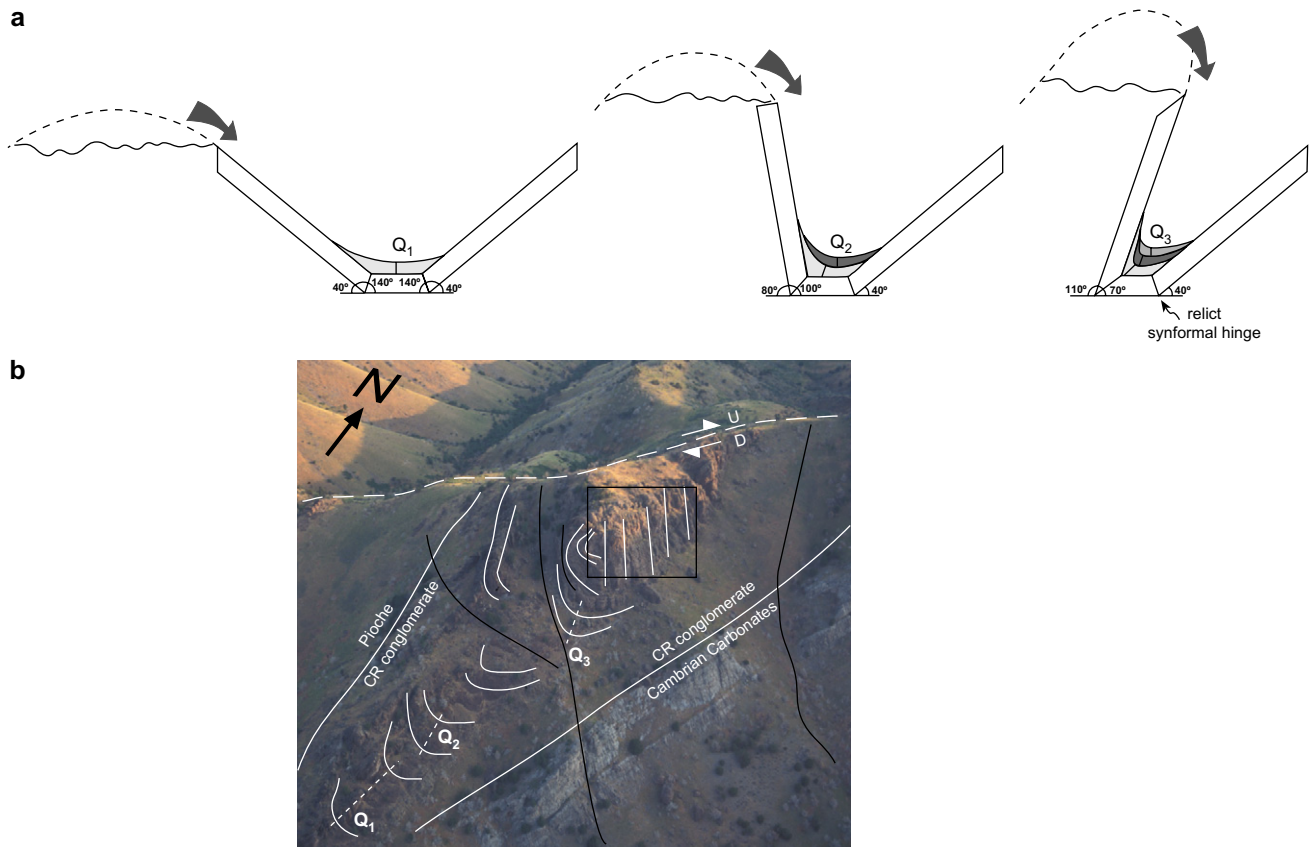


Fig. 8. (a) Schematic cross-sectional model of the CR anticline–syncline pair showing progressive fold-tightening and deposition for different layers ($Q_1 - Q_3$; Q_1 is the oldest) of the CR synorogenic conglomerate. (These layers are all part of the Kcq2 unit from Lawton et al. (1997)). Dashed line illustrates eroded portion of adjoining anticline. Each successive layer is deposited at the lowest structural elevation within the synclinal hinge. (b) Oblique aerial photograph (from low flying aircraft) of the core of the syncline showing the Cambrian carbonate/CR synorogenic conglomerate contact and the Pioche/CR synorogenic conglomerate contact (solid white line), macro-scale faults (black lines), transverse zone (dashed white line), and the folded conglomerate layers, labeled $Q_1 - Q_3$. Boxed area shows location of Fig. 9. White vertical lines in boxed area highlight the EW trending fracture sets preserved in the conglomerate; these are illustrated more clearly in Fig. 9b.

than creating new fracture sets in the Pioche quartzite; less energy is required to reactivate pre-existing surfaces than to create new surfaces to slide on (Donath, 1961; Sibson, 1985; Twiss and Moores, 1992). From this model, it can be said that the argillite strongly influenced the fold shape during these stages of fold-tightening.

Beyond a limb dip of 80° (interlimb angle < 60°), the fractures and cleavage surfaces were rotated into positions where a minimum of three fracture and three cleavage sets were reactivated to accommodate vertical limb thinning and stretching (Fig. 11d). So, based on the model shown in Fig. 11d, in the later stages of fold-tightening, the quartzite and argillite members equally influenced the Pioche fold's geometry.

Many models predict that once a fold reaches limb dips of ~60° (interlimb angle of ~60°), the fold 'locks' because the competent limbs can no longer rotate (Ramsay, 1974; Williams, 1980). Several models also suggest that beyond this 'locking' point, the incompetent member controls the folding process (Ramsay, 1974; Williams, 1980). The natural case study modeled here suggests a slightly different scenario. There does not appear to be a 'locking point', but

instead a gradual change between limb dips of 40° and 60° (i.e., between an interlimb angle of 100° and 80°) during which the argillite controlled the fold geometry. However, at a limb dip of ~80° and steeper (interlimb angle < 60°), the *function* of cataclastic flow throughout the entire Pioche unit switched from accommodating E-W shortening to ~vertical extension.

Slickenlines are found within beds that are dipping steeper than 60° (Figs. 5a, 11c); therefore, fracture reactivation in the later stages (>60° limb dips) of fold tightening resulted in the late-stage slickenlines preserved in the west limb. Based on the orientation of the fractures and cleavages, and the slickenlines on those surfaces, we can surmise that as folding progressed, argillite migrated from the limbs to the hinge (Fig. 11d). Late stage argillite migration may have induced the formation of FPFs in the hinge region to accommodate the excess volume of material. At the same time, the Pioche quartzite layers moved closer together in the limbs as the argillite moved from the limbs to the hinge. This adjustment was assisted by reactivating early LPS fracture sets, which accommodated vertical limb-thinning and extension, rather than E-W shortening (Fig. 11d).

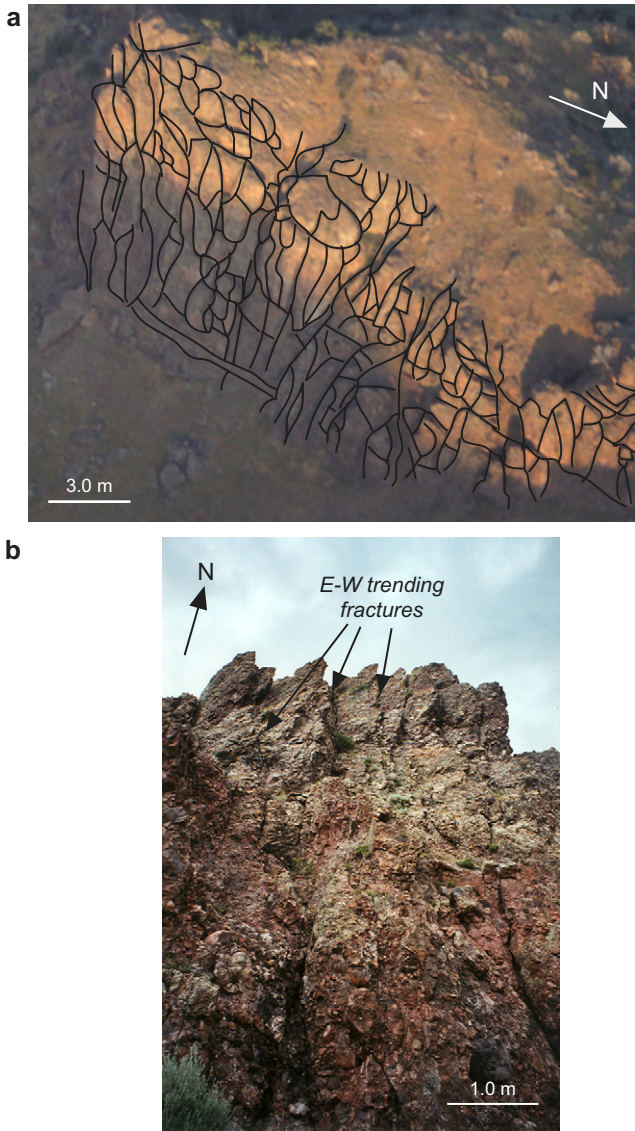


Fig. 9. Fracture patterns preserved in the CR synorogenic conglomerate showing the $\sim 1 \text{ m}^3$ blocks defined by three major sets of fractures (steeply dipping sets trending NS, EW and S 30° W). This fractured region of the conglomerate overlies the folded units and corresponds to the Kcq3 layer of Lawton et al. (1997). (b) A close up view of the EW trending fracture sets, the youngest of the three sets.

This scenario for late stage reactivation and argillite migration is suggested by the orientation of the FPF fold axis and the pole to the motion plane (M-pole), which is defined by the slickenlines; both plunge $\sim 10^\circ$ due north, which is gentler than the first-order syncline axis ($32^\circ, 337^\circ$). In other words, these structures were not present during the CR syncline's entire folding history. The first-order fold is interpreted to have had a plunge of $\sim 20^\circ$ when the FPF formed and the fracture-bound quartzite blocks started to slide past each other. Previous work done in the CR syncline (Lawton et al., 1997), suggests that the fold had already tightened beyond an interlimb angle of 100° by the time the fold developed a plunge of $\sim 20^\circ$. So, these folding related structures formed in the late/intermediate stages of fold-tightening. Moreover,

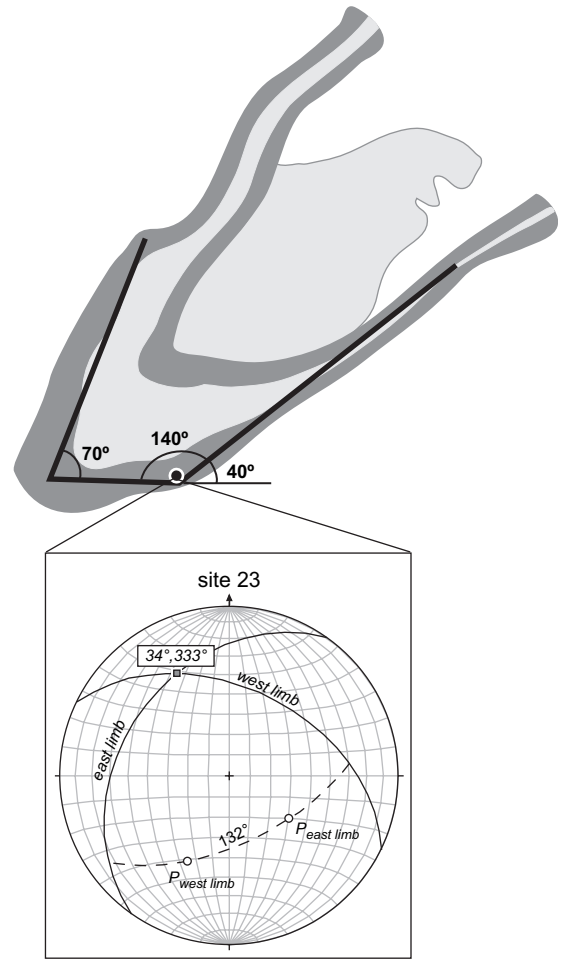


Fig. 10. Down-plunge projection of the core of the CR syncline with stereogram showing relict synformal hinge orientation, preserved at site 23. Thick black great circles on the stereogram are the average bedding orientations of the east and west limbs. The fold's interlimb angle is the small circle measured between bedding, drawn through the bedding poles ($P_{\text{west limb}}$ and $P_{\text{east limb}}$), and is 132° . The box-fold geometry is highlighted as the thick black lines on the down-plunge projection. (b) White solid lines define the Pioche unit. White dot shows location of site 23.

since the orientations of the FPF and M-pole are nearly identical, we interpret they formed during the *same* intermediate/late stage of fold-tightening.

The thickness of the Pioche argillite is thicker in the west limb than it is in the east limb (Fig. 6a), which may appear to be counter-intuitive. Since the west limb underwent more active rotation than the east limb, it can be expected that the west limb would have extended and thinned more, with more argillite migration to the hinge. However, as the fold tightened and space problems increased in the hinge region, some of the excess argillite in the hinge region may have re-migrated into the limbs. During the later stages of fold-tightening, three cleavage surfaces were in positions for reactivation in the west limb, while only two sets were in positions for reactivation in the east limb (Fig. 11b,d). Because the east limb did not have a sufficient number of active cleavage surfaces, the re-migration may have concentrated into the west limb, thereby increasing the thickness of the Pioche argillite

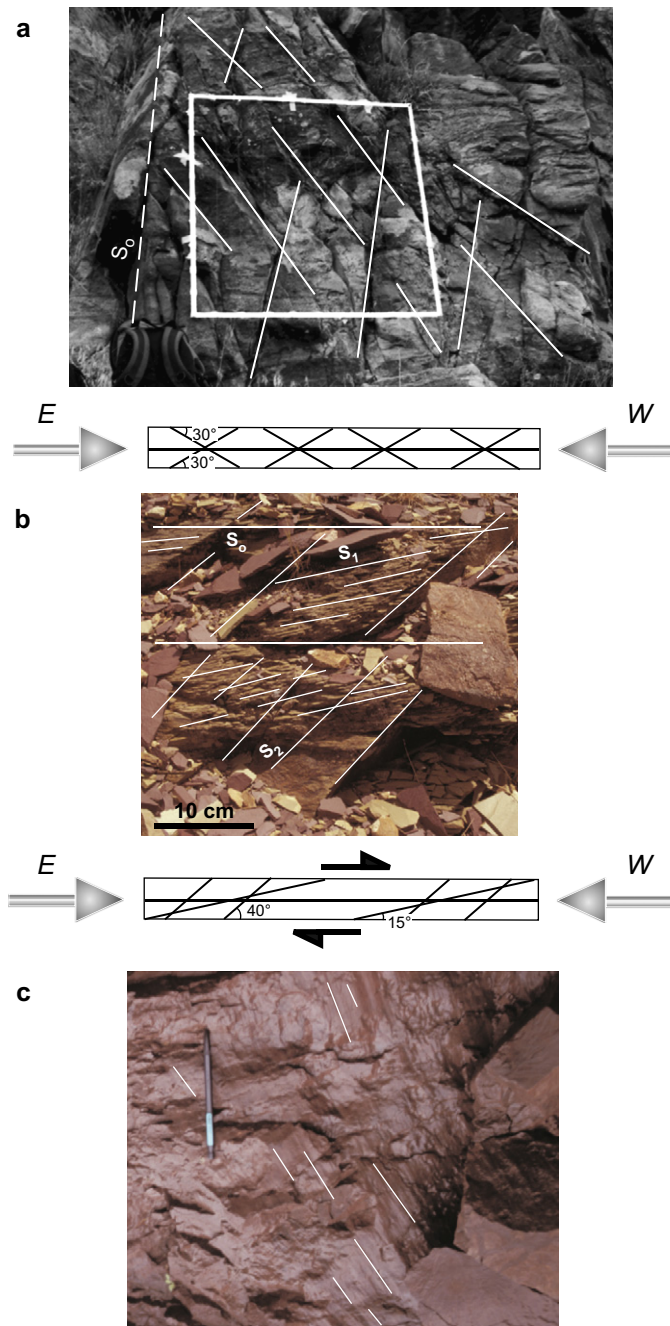


Fig. 11. (a) Outcrop-scale photo of the Pioche quartzite showing LPS conjugate–conjugate fracture sets (solid white lines) dipping $\sim 30^\circ$ from bedding (dashed white line labeled S_0). Two-dimensional schematic model of fracture development in quartzite layers. The two arrows depict an EW sub-horizontal shortening direction. (b) Outcrop-scale photo showing bedding (S_0) and two sets of cleavage surfaces (S_1 dipping 15° from bedding and S_2 dipping 40° from bedding) preserved in the Pioche argillite. Two-dimensional schematic model suggesting that cleavage developed pre-folding, under an east-directed shear sense. (c) Photograph, looking towards 245° , of slickenlines preserved on a cleavage surface ($69^\circ, 071^\circ$) within the Pioche formation. Bedding orientation is $82^\circ, 085^\circ$. (d) Graph and two-dimensional schematic model for fold tightening of the Pioche quartzite and argillite. Reactivated fracture/cleavage sets that accommodate E-W shortening are shown as thick, black lines while reactivated fracture/cleavage sets that accommodate vertical extension are shown as thin, gray lines. A minimum of three fracture/cleavage sets is required for three-dimensional (block controlled) cataclastic flow. The number of fracture sets reactivated is illustrated with horizontal bars on the graph.

layer in the west limb of the CR syncline. Alternatively (and more likely), the argillite may have thickened there if the section was repeated during early CR thrusting (Fig. 11d). This model agrees with published balanced cross-sections constructed for stratigraphic units adjacent to the Pioche in the CR syncline (Lawton et al., 1997; Mitra and Sussman, 1997). Unfortunately, the argillite is poorly exposed and therefore, we are unable to reach an unequivocal interpretation.

5.2.3. Flexural slip

During stages of bed-parallel flexural slip, bedding-plane lineations may form sub-perpendicular to the hinge of the fold. Asymmetric parasitic folds, particularly in thin-bedded units with alternating strong and weak layers, such as the Pioche quartzites and argillites, may also form. Evidence for this bed-parallel flexural slip is preserved in the slickensides and parasitic folds in the Pioche quartzite.

The lineations on the Pioche quartzite bedding surfaces and LPS conjugate–conjugate fracture sets are sub-perpendicular to the fold hinge (Fig. 5a). So, block-controlled cataclastic flow within the quartzite layers not only accommodated bed thickness changes, but also bed-parallel flexural slip, during the later stages of fold tightening.

The z-fold (looking north) is preserved within the east limb of the lower quartzite and has asymmetry consistent with flexural slip (Fig. 6a). The z-fold plunges 12° towards 358° , nearly identical to the orientation of the FPF (Fig. 6a,c) and the slickenlines average M-pole (Fig. 5a,b). Based on its plunge, we interpret the z-fold formed at the same time as the FPF and slickenlines. So, flexural slip assisted the later stages of fold-tightening.

In addition to flexural slip, the z-fold supplies further evidence for hinge migration (Fig. 6a). Based on the plunges of both the eastern synformal hinge and the z-fold, we have surmised that the eastern synformal hinge formed early and the z-fold formed in the later stages of fold-tightening. When the z-fold formed, the small (eastern) synformal hinge had already moved into the east limb of the first-order CR syncline and was a relict, inactive structure. The z-fold formed west of this relict synformal hinge, but in the east limb of the first-order CR syncline (Fig. 6a).

5.3. Microscale analysis

‘Unfractured’ (which may include rocks with *healed* fractures) to intensely fractured and cataclastic rocks were studied in thin sections under a microscope using ImagePro Plus, a Microsoft Windows based image analysis software package. This program counted unfractured grains and fractured clasts, and determined the area, perimeter, axial ratio, best-fit ellipse, and shape orientation of each grain/clast; the data was then analyzed using Excel (Fig. 12).

Unfractured grains in the Pioche quartzite have a relatively unimodal grain size (Fig. 13). The early plastic strain in these quartzites is relatively small (Fry strain ellipse axial ratios < 1.2) (Fry, 1979; Ismat and Mitra, 2001a); the dominant mode of deformation was within the EF regime. The fractured areas of the Pioche quartzites contain intra-, inter-, and trans-

d

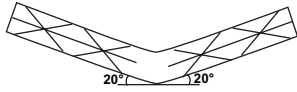
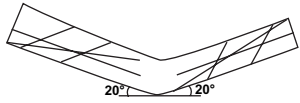
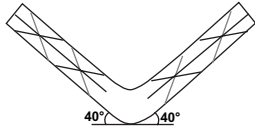
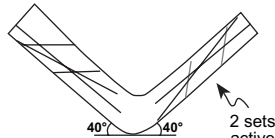
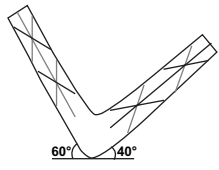
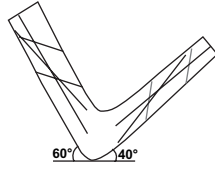
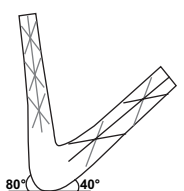
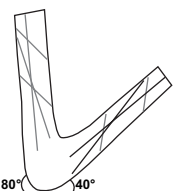
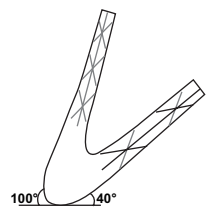
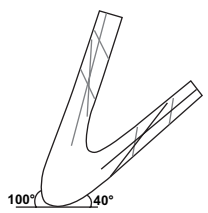
Pioche quartzite active fracture sets			Pioche argillite active cleavage sets		
number of active fracture sets (w-limb)		two-dimensional model	number of active cleavage sets (w-limb)		two-dimensional model
EW shortening	3		EW shortening	3	
vertical extension			vertical extension		
EW shortening	2		EW shortening	3	
vertical extension	1		vertical extension		
EW shortening	1		EW shortening		
vertical extension	2		vertical extension	3	
EW shortening			EW shortening		
vertical extension	3		vertical extension	3	
EW shortening			EW shortening		
vertical extension	3		vertical extension	3	

Fig. 11. (continued)

granular fractures. In some places, the fracturing increased to such a degree that well-developed cataclastic zones formed, some of which are foliated.

Outcrop-scale fractures/zones are produced by the linkage of microscale fractures/zones (Twiss and Moores, 1992; Ismat and Mitra, 2001a). So, deformation preserved at the microscale records mesoscale activity, such as the number of deformation episodes. Evidence for shearing of mesoscopic fracture-bound blocks past each other is preserved in

cataclasite zones at the microscale. Well-developed cataclasite zones are rarely cross-cut by other cataclasite zones. In addition, finer grained cataclasite zones follow coarser grained zones, implying that the coarser grained zones are older and were reactivated. This suggests that very few, if any, new fracture sets were produced during folding. In other words, it reconfirms the mesoscale data, which showed that the initial LPS fracture sets were selectively reactivated as folding progressed.

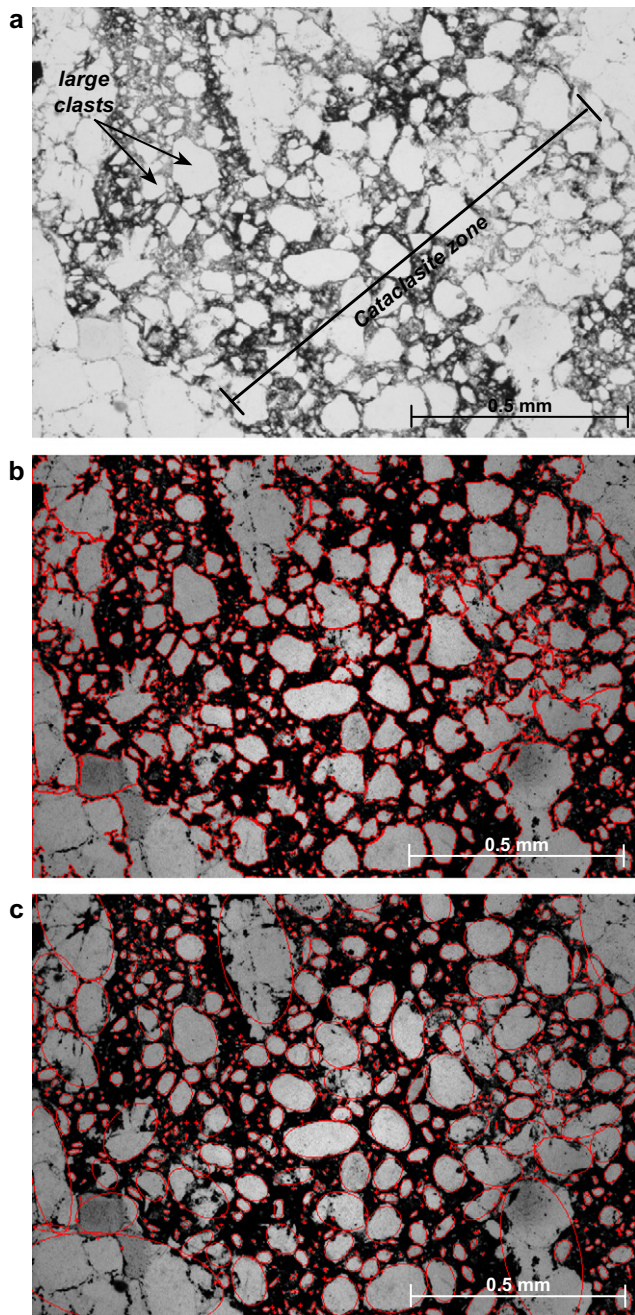


Fig. 12. (a)–(c) Photomicrograph of Pioche quartzite from site 10 showing range in grain/clast size within a well-developed cataclasite zone. (b),(c) contrast enhanced for grain/clast analysis with ImagePro Plus. (a) Plane-polarized view. Note large grains/clasts surrounded by a ‘moat’ of medium sized shard like clasts. (b) Grain/clast outlines measured. (c) Best fit ellipses drawn.

Fractured microscale clast morphology ranges in shape, size, and axial ratio. In general, the fractured clasts were sub-angular to very angular and have a trimodal size distribution (Fig. 14). The clasts are grouped into *large* (9000–80,000 μm^2), *medium* (700–9000 μm^2), and *small* (30–700 μm^2) size ranges (Fig. 14). Large clasts have lower axial ratios, with a mean of 1.7 ± 0.1 . Medium-sized clasts have higher average axial ratios of $\sim 2.3 \pm 0.2$, while the small clasts have a mean axial ratio of 2.0 ± 0.1 (Fig. 14).

Orientations of the long axes of the microscale fractured clasts do not have clear, consistent orientations. Unlike the microscale clasts, the outcrop-scale fracture-bound block axes have a consistent orientation at each site, with the maximum shortening direction \sim parallel to the long axes (Ismat and Mitra, 2005b); so strain patterns at the mesoscale can be determined.

The largest clasts fractured with through-going intra-granular cracks. Some of these fractures propagated at high angles to the major axes of the clasts; this portion of the clast has the largest radius of curvature, and therefore, is most likely to develop fractures at high angles to the surface. Intra-granular cracks also broke off jagged/irregular edges of these large grains, forming splinter-like ‘shards’; these shards form the medium-sized grains. Due to their ‘splinter-like’ shape, the medium sized clasts have the highest axial ratios (Fig. 14). These medium-sized clasts were further broken down as through-going intra-granular fractures split these clasts in half, approximately perpendicular to their major axes. This continued breakdown of the medium sized clasts resulted in the formation of the smallest clast size. Once the smallest clasts reached a size of $\sim <30 \mu\text{m}^2$, the high surface area/volume ratio suppressed further fracture (i.e. Hall–Petch relationship). Clast areas that were too small to be deciphered are considered here to be ‘matrix’.

Large clasts are rarely found in contact with other large clasts; they tend to be surrounded by the medium-size grains (Fig. 12). The long axes of the medium sized clasts are typically oriented approximately parallel to the surface of the large clast they broke off from, and so do not produce stress concentrations along the surface of the large grains. This ring of medium-sized clasts essentially ‘buffered’ the largest clasts, thereby preventing intra-granular fractures from breaking these large clasts down any further (Rawling and Goodwin, 2002). So, large relict clasts are typically surrounded by a ‘moat’ of medium-sized shards, which are further surrounded by the smallest clast size and matrix (Fig. 12).

Although fracturing and cataclasis took place at all scales, the manner of fracturing and the resulting morphological characteristics of the fractured areas vary across scales. So, even though the EF mechanisms are active at all scales, the *style* of deformation is not scale-independent.

6. Summary of kinematic history

The kinematic history for folding of the CR syncline based on analysis and interpretation of structures preserved throughout the fold is summarized below.

1. Early LPS cleavage surfaces form in the Pioche argillite and conjugate–conjugate fracture sets form in the Pioche quartzite, both when the Pioche Formation was sub-horizontal.
2. Up to limb dips of $\sim 40^\circ$ (i.e. $\sim 100^\circ$ interlimb angle), the competent Pioche quartzite controls the folding process. Limb rotation is assisted by block-controlled cataclastic

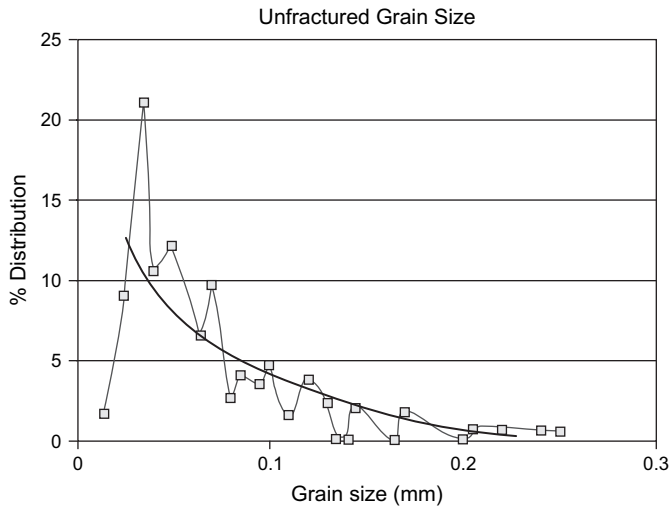


Fig. 13. Plot of percent distribution versus grain size of unfractured Pioche quartzite, as viewed at the microscale. Grain size (length of grain measured in mm) was determined using Spektor Chord analyses (Underwood, 1970). Thirty-one samples were measured along 4–6 transects through each sample. There is a fairly uniform distribution of a small range in grain size. The average length of an unfractured Pioche quartzite grain is ~ 0.12 mm.

flow by reactivating the early LPS conjugate–conjugate fracture sets.

3. The Pioche sustains a double-kink box-fold geometry until $\sim 40^\circ$ limb dips ($\sim 100^\circ$ interlimb angle). At this point, the hinge farther to the west remains active while the eastern hinge is preserved as a relict synformal hinge within the east limb of the CR syncline. The CR syncline continues to tighten by rotation and thinning of the west limb; the east limb maintains a dip of $\sim 40^\circ$.
4. The fold had already tightened beyond an interlimb angle of 100° by the time the fold developed a plunge of $\sim 20^\circ$
5. Between limb dips of $\sim 40^\circ$ and $\sim 60^\circ$ (interlimb angles between $\sim 100^\circ$ and 80°), an insufficient number and orientation of fracture sets are reactivated to thoroughly deform the competent quartzite by cataclastic flow. During these stages, the incompetent argillite member controls the folding process. The Pioche argillite continues to flow from the limbs to the hinge, and is accommodated by block-controlled cataclastic flow as rhomb-shaped blocks of argillite slide past each other along LPS cleavage surfaces. Many folding models suggest that at 60° limb dips (i.e., 60° interlimb angle), there is a shift from the competent to the incompetent member controlling the folding process. The natural case study presented here, however, suggests that the shift may be more gradual and takes place over a range of limb dips.
6. In the later stages of fold tightening ($>60^\circ$ limb dips), the Pioche argillite flows from the limbs to the hinge and fault-propagation folds form in response to this excess volume in the hinge region. In addition, a few selected fracture sets in the Pioche quartzite are activated as sliding surfaces to accommodate limb thinning and flexural slip, resulting in late stage slickenlines on these fracture surfaces.

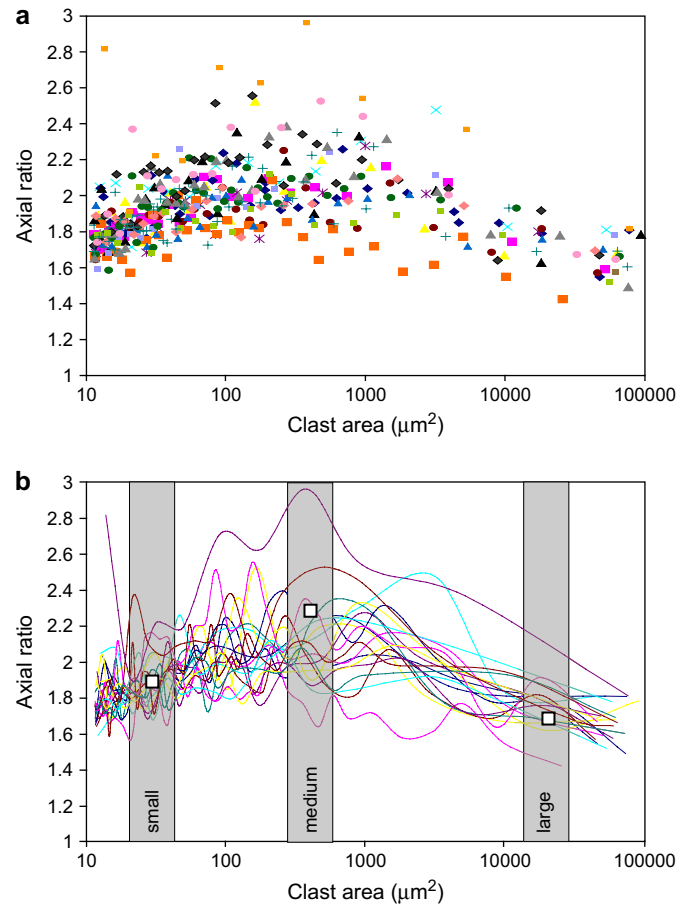


Fig. 14. Microscale fractured clast morphology plotted in terms of axial ratio vs. log of clast area; these dimensions were measured using ImagePro Plus. Nineteen rock samples, each from a different site throughout the Pioche quartzite, were analyzed. Each sample is plotted as (a) a unique symbol on the scatter plot and (b) as a curve with a different shade of gray. Three mutually perpendicular thin sections were cut and analyzed from each sample. The graphs for the 19 samples represent data collected from 57 thin sections, with ~ 2000 clasts/grains counted from each thin section. (b) Trimodal clast distribution (large, medium and small) is identified from the three main peaks. A white box marks the average of each clast area and axial ratio.

7. At limb dips $>80^\circ$ ($<60^\circ$ interlimb angle), the quartzite and the argillite members contributed equally to the folding process.
8. The steeply dipping E-W fracture sets in the synorogenic conglomerate are late stage features. These fractures cross cut all other fracture sets and folds in the conglomerate. Since these fractures are \sim vertical, we surmise that they formed after the CR syncline had developed a plunge of $\sim 32^\circ$. Unlike the Pioche quartzite, the CR conglomerate formed new fractures during the later stages of fold-tightening; this may be because the conglomerate did not have older, preferentially oriented fractures that could be reactivated.
9. Finally, \sim vertical, E-W trending macroscale faults formed. These are the last structures formed, and cut across the entire fold core (in map view). These faults cross-cut all other fracture sets in the synorogenic conglomerate, the Pioche unit, the Cambrian limestone and

the upper Tintic quartzite, as well as the folds in the conglomerate. They may have formed as result of longitudinal splitting with an overall east-west maximum shortening direction and/or extension parallel to the hinge during fold-tightening.

7. Discussion

Folds formed by different folding mechanisms might undergo distinctive physical processes during their growth, but the resulting strain distributions may be similar (Ramsay, 1967). Because of this, trying to get at the forces that were active during folding may be nearly impossible. We have focused on the geometry of folds because that is what can be observed. The geometry of natural folds is frequently compared to physical, theoretical and/or computer models produced in the lab to help unravel complicated fold related structures. However, these models often fall short due to simplifying assumptions and limited variables that can be tested and/or adjusted.

Therefore, a useful approach to understanding folding processes is to carefully examine natural folds and to evaluate the kinematics implied by various mesoscopic and microscopic fold-related structures. Unfortunately, in folds that formed by plastic deformation mechanisms (i.e., within the quasi-plastic regime), the folding history may be partly obscured by high temperature recrystallization or other healing mechanisms. Folds that formed within the EF regime have potential for preserving evidence of successive stages as structures formed during each stage of deformation cross-cut those formed during earlier stages. So, the evolution of folds developed within the EF regime can be well tracked and the kinematic history can then be applied to a wide range of natural folds formed under similar conditions. Moreover, unraveling the kinematic details of natural folds can be used to better understand folding models; unusual structures that develop in these models that were once ignored may now be viewed as real, and vice versa.

The kinematic details of the CR syncline agree with features of many folding models. For example, models have shown that less energy is expended in sliding along pre-existing surfaces than in forming new surfaces to slide on (e.g. Schmid's law) (Paterson, 1978; Bles and Feuga, 1986; Twiss and Moores, 1992). And, discontinuous surfaces, such as fractures, may not only be reactivated, but their function in the folding process can change (Bott, 1959; Donath, 1961; Price, 1967; Sibson, 1985; Bles and Feuga, 1986; Ismat and Mitra, 2001a).

We have also found how natural folds may stray from the geometry of modeled folds in the following ways. First, the Pioche unit may have had multiple pinning points, in different locations during different stages of folding. In the early stages of folding, when the Pioche unit had a box-fold geometry, both of the kink hinges were presumably pinned. Beyond 40° limb dips, only the western-most hinge remained active; the other hinge was no longer pinned and formed part of the east limb of the first-order fold. Second, a fold's hinge may migrate

and the style of migration may also vary up and down through a folded sequence, as it does in the CR syncline from the Pioche unit to the older Proterozoic quartzites below. Third, parasitic folds can form as intermediate/late stage structures, as they did in the Pioche quartzite, rather than just early buckling and then flexural slip related features. Finally, existing models suggest that at an interlimb angle of ~60° (i.e., limb dips of ~60° for upright, symmetrical folds), the folding process changes whereby the incompetent member takes over from the competent member as the controlling unit in the folding process (Dieterich, 1970; Ramsay, 1974; Williams, 1980). The kinematic history of the natural fold presented here, however, suggests that between limb dips of 40° and 60° (i.e., between interlimb angles of 100° and 80°), the incompetent Pioche argillite strongly influenced the geometry of the fold. At ~80° limb dips (~60° interlimb angle), however, the role of the fractures and cleavage surfaces changed. LPS fractures and cleavage surfaces that were originally used to accommodate shortening were later reactivated to assist vertical stretching and limb thinning. So, beyond 80° limb dips the competent and incompetent layers contributed equally to the folding process.

Although models are useful for first-order interpretations of folds, details of the natural complexities associated with fold development are often overlooked. Based on the natural case study analyzed here, we have attempted to show that tracking the evolution of structures produced in a natural fold can provide critical details that may be overlooked and/or oversimplified in established folding models. As a result, the kinematic details unraveled from a natural fold can improve our understanding of established multilayer fold models, and aid in the construction of more advanced models.

8. Conclusions

1. Beyond limb dips of ~40° (interlimb angle of 100°), the fold geometry dramatically changed. The early double-kink fold shape was modified to a single hinge fold. Fold-tightening continued by rotation, thinning and stretching of the west-limb; this change at 100° is commonly observed in both buckle and bend folds whereby the characteristic mechanisms distinguishing these two types of folds break down.
2. The Pioche unit's fold shape adjustment mimics the geometry of the rest of CR syncline. However, the style of hinge migration and activity varies up and down through the stratigraphic succession within the CR syncline, and may be a function of lithological controls.
3. Elastico-frictional mechanisms, such as fracturing and cataclastic flow, are preserved at multiple scales. The style of deformation, however, varies across scales and is a function of *matrix-controlled* versus *block-controlled* cataclastic flow.
4. Between limb dips of ~40° and ~60° (i.e., between interlimb angles of 100° and 80°), the fold-shape controlling member changed progressively from the competent Pioche quartzite to the incompetent Pioche argillite.

Many multi-layer folding models predict this switch at 60° limb dips (interlimb angle of 60°).

5. The CR syncline relieved space problems developed in the core during fold-tightening by hinge migration, bed thickness changes, out-of-core thrusting, and varying the originally incompetent argillite and competent quartzite members as controlling the folding process, both spatially and temporally.
6. Parasitic folds preserved in the hinge region of the Pioche unit in the CR syncline formed during the later stages of fold-tightening. This is unusual; most models for folding suggest that parasitic folds form in the early stages of folding.
7. The earliest formed LPS conjugate–conjugate fractures in the Pioche quartzite and the LPS cleavage surfaces in the Pioche argillite were passively rotated and later reactivated during fold-tightening in order to accommodate vertical stretching and thinning of the rotated west limb.
8. A high density of late stage fractures may not have formed in the Pioche quartzite because folding may have continued by bed-parallel flexural slip along weak argillite layers and reactivation of older fractures.

Acknowledgements

Two Franklin and Marshall College COG awards given to Z. Ismat, and a Franklin and Marshall College Hackman scholarship and Leser grant awarded to B. Benford supported this research. We thank the reviewers, Adolph Yankee and Charles Onasch, and especially the editor Bill Dunne, for their detailed comments, which were very useful in improving the paper. We also thank Gautam Mitra and Don Fisher for helpful discussions and comments on an earlier version of this paper. Finally, we would also like to thank P. Riley for his assistance in the field.

References

- Allmendinger, R.W., Sharp, J.W., Von Tish, D., Serpa, L., Brown, L., Oliver, J., Kaufman, S., Smith, R.B., 1983. Cenozoic and Mesozoic structure of the Eastern Basin and Range province, Utah, from COCORP seismic reflection data. *Geology* 11, 532–536.
- Armstrong, R.L., 1968. Sevier orogenic belt in Nevada and Utah. *Geological Society of America Bulletin* 79, 429–458.
- Atkinson, B.K. (Ed.), 1989. *Fracture Mechanics of Rock*. Academic Press.
- Bayly, M.B., 1974. An energy calculation regarding the roundness of folds. *Tectonophysics* 24, 291–316.
- Biot, M.A., 1957. Folding instability of a layered visco-elastic medium under compression. *Proceedings of the Royal Society of London A242*, 444–454.
- Biot, M.A., 1959b. On the instability and folding deformation of a layered visco-elastic medium in compression. *Applied Mechanics* 26, 393–400.
- Biot, M.A., 1961. Theory of folding of stratified visco-elastic media and its implications in tectonics and orogenesis. *Geological Society of America Bulletin* 72, 1595–1620.
- Biot, M.A., 1965. Theory of similar folding of the first and second kind. *Geological Society of America Bulletin* 76, 371–381.
- Bles, J.L., Feuga, B., 1986. *The Fracture of Rocks* (translated by Wanklyn, J.). Elsevier.
- Bott, M.H.P., 1959. The mechanics of oblique slip faulting. *Geology Magazine* 96, 109–116.
- Chapple, W.M., 1969. Fold shape and rheology: the folding of an isolated, viscous-plastic layer. *Tectonophysics* 7, 97–116.
- Christiansen, R.F., 1952. Structure and stratigraphy of the Canyon Range, Utah. *Geological Society of America Bulletin* 63, 717–740.
- Christie-Blick, N., 1982. Upper Proterozoic and Lower Cambrian rocks of the Sheeprock Mountains, Utah: regional correlation and significance. *Geological Society of America Bulletin* 93, 735–750.
- Cooke, M.L., Mollema, P.N., Pollard, D.D., Aydin, A., 2000. Interlayer slip and joint localization in the East Kaibab Monocline, Utah: field evidence and results from numerical modelling. In: Cosgrove, J.W., Ameen, M.S. (Eds.), *Forced Folds and Fractures*. Geological Society, London, Special Publications, vol. 169, pp. 23–49.
- DeCelles, P.G., Lawton, T.F., Mitra, G., 1995. Timing of Sevier thrusting, central Utah. *Geology* 23, 699–702.
- Dieterich, J.H., 1970. Computer experiments on mechanics of finite amplitude folds. *Canadian Journal of Earth Sciences* 7, 467–476.
- Dieterich, J.H., Carter, N.L., 1969. Stress history of folding. *American Journal of Science* 267, 129–154.
- Donath, F.A., 1961. Experimental study of shear failure in anisotropic rocks. *Geological Society of America Bulletin* 72, 985–989.
- Elliott, D., 1976a. The energy balance and deformation mechanisms of thrust sheets. *Philosophical Transaction of the Royal Society London Series A* 283, 289–312.
- Fletcher, R.C., 1977. Folding of a single viscous layer: exact infinitesimal amplitude solution. *Tectonophysics* 39, 593–606.
- Fry, N., 1979. Random point distributions and strain measurements in rocks. *Tectonophysics* 60, 89–115.
- Ghosh, S.K., 1966. Experimental tests of buckling folds in relation to the strain ellipsoid in simple shear deformation. *Tectonophysics* 3, 169–185.
- Hadizadeh, J., Rutter, E.H., 1983. The low temperature Brittle-Ductile transition in a quartzite and the occurrence of cataclastic flow in nature. *Geologische Rundschau* 72, 493–509.
- Handin, J.W., Friedman, M., Logan, J.M., Pattison, L.J., Swolfs, H.S., 1972. Experimental folding of rocks under confining pressure: buckling of single layer rock beams. *American Geophysics Union Monograph* 16, 1–28.
- Hintze, L.F., 1988. Geologic history of Utah. *Brigham Young University Geology Studies Special Publication* 7, p. 202.
- Hirth, G., Tullis, J., 1994. The brittle-plastic transition in experimentally deformed quartz aggregates. *Journal of Geophysical Research* 99, 11731–11747.
- Hobbs, B.E., Means, W.D., Williams, P.F., 1976. *An Outline of Structural Geology*. John Wiley and Sons, New York.
- Hudleston, P.J., 1973b. An analysis of ‘single layer’ folds developed experimentally in viscous media. *Tectonophysics* 16, 189–214.
- Ismat, Z., Mitra, G., 2001a. Folding by cataclastic flow at shallow crustal levels in the Canyon Range, Sevier orogenic belt, west-central Utah. *Journal of Structural Geology* 23, 355–378.
- Ismat, Z., Mitra, G., 2005a. Fold-thrust belt evolution expressed in an internal thrust sheet, Sevier orogeny: the role of cataclastic flow. *Geological Society of America Bulletin* 117, 764–782.
- Ismat, Z., Mitra, G., 2005b. Folding by cataclastic flow: evolution of controlling factors during deformation. *Journal of Structural Geology* 27, 2181–2203.
- Johnson, A.M., 1977. *Styles of Folding: Mechanics and Mechanisms of Folding of Natural Elastic Materials*. Elsevier.
- Lawton, T.F., Sprinkel, D.A., DeCelles, P.G., Mitra, G., Sussman, A.J., Weiss, M.P., 1997. Stratigraphy and structure of the Sevier thrust belt and proximal foreland-basin system in central Utah: a transect from the Sevier Desert to the Wasatch Plateau. *BYU Geology Studies* 42, 33–67.
- Lisle, R.J., 2000. Predicting patterns of strain from three-dimensional fold geometries: Neutral surface folds and forced folds. In: Cosgrove, J.W., Ameen, M.S. (Eds.), *Forced Folds and Fractures*. Geological Society, London, Special Publications, vol. 169, pp. 213–221.
- Marshak, S., Geiser, P.A., Alvarez, W., Engelder, T., 1982. Mesoscopic fault array in the northern Umbrian Apennine fold belt, Italy: geometry of

- conjugate shear by pressure solution. *Geological Society of America Bulletin* 93, 1013–1022.
- Marshak, S., Mitra, G., 1988. *Basic Methods of Structural Geology*. Prentice-Hall, Englewood Cliffs, NJ.
- Mitra, G., 1997. Evolution of salients in a fold-and-thrust belt: the effects of sedimentary basin geometry, strain distribution and critical taper. In: Sengupta, S. (Ed.), *Evolution of Geological Structures in Micro- to Macro-scales*. Chapman & Hall, London, pp. 59–90.
- Mitra, G., Ismat, Z., 2001. Microfracturing associated with reactivated fault zones and shear zones: what can it tell us about deformation history? In: Holdsworth, R.E., Strachan, R.A., Magloughlin, J.F., Knipe, R.J. (Eds.), *The Nature and Tectonic Significance of Fault Zone Weakening*. Geological Society, London, Special Publications, vol. 186, pp. 113–140.
- Mitra, G., Sussman, A.J., 1997. Structural evolution of connecting splay duplexes and their implications for critical taper: an example based on geometry and kinematics of the Canyon Range culmination, Sevier belt, Central Utah. *Journal of Structural Geology* 19, 503–521.
- Neurath, C., Smith, R.B., 1982. The effect of material properties on growth-rates of folding and boudinage: experiments with wax models. *Journal of Structural Geology* 4, 215–229.
- Paterson, M.S., 1978. *Experimental Rock Deformation – The Brittle Field*. Springer-Verlag.
- Price, N.J., Cosgrove, J.W., 1990. *Analysis of Geological Structures*. Cambridge University Press.
- Price, R.A., 1967. The tectonic significance of mesoscopic subfabrics in the southern Rocky mountains of Alberta and British Columbia. *Canadian Journal of Earth Sciences* 4, 39–70.
- Ramberg, H., 1960. Relationships between lengths of arc and thickness of pygmatically folded veins. *American Journal of Science* 258, 36–46.
- Ramberg, H., 1963a. Strain distribution and geometry of folds. *Bulletin of the Institute of Geology University of Uppsala* 42, 1–20.
- Ramberg, H., 1964. Selective buckling of composite layers with contrasted rheological properties: a theory for simultaneous formation of several orders of folds. *Tectonophysics* 1, 307–341.
- Ramsay, J.G., 1967. *Folding and Fracturing of the Rocks*. McGraw-Hill.
- Ramsay, J.G., 1974. Development of chevron folds. *Geological Society of America Bulletin* 85, 1741–1754.
- Rawling, G.C., Goodwin, L.B., 2002. Cataclasis and particulate flow in faulted, poorly lithified sediments. *Journal of Structural Geology* 25, 317–331.
- Reches, Z., 1983. Faulting of rocks in three-dimensional strain fields: II. Theoretical analysis. *Tectonophysics* 95, 133–156.
- Rutter, E.H., 1986. On the nomenclature of mode of failure transitions in rocks. *Tectonophysics* 122, 381–387.
- Sibson, R.H., 1977. Fault rocks and fault mechanisms. *Journal of the Geological Society (London)* 133, 191–213.
- Sibson, R.H., 1985. A note on fault reactivation. *Journal of Structural Geology* 7, 751–754.
- Sherwin, J., Chapple, W.M., 1968. Wavelengths of single-layer folds; a comparison between theory and observation. *American Journal of Science* 266, 167–179.
- Summers, J.M., 1979. An experimental and theoretical investigation of multi-layer fold development. PhD thesis, University of London.
- Treagus, S., 1983. A theory of finite strain variation through contrasting layers, and its bearing on cleavage refraction. *Journal of Structural Geology* 5, 351–368.
- Twiss, R.J., Moores, E.M., 1992. *Structural Geology*. W.H. Freeman and Company, New York.
- Underwood, E.E., 1970. *Quantitative Stereology*. Addison-Wesley Publishing Company.
- Williams, J.R., 1980. Similar and chevron folds in multilayers, using finite element and geometric models. *Tectonophysics* 65, 323–338.
- Wojtal, S., 1989. Measuring displacement gradients and strains in rocks. *Journal of Structural Geology* 11, 669–678.